ELSEVIER

Journal of Non-Crystalline Solids 224 (1998) 259–266

JOURNAL OF NON-CRYSTALLINE SOLIDS

Tin oxide gel shrinkage during CO_2 supercritical drying

S.-Yen Wang, Nae-Lih Wu *

Department of Chemical Engineering, National Taiwan University, Taipei, Taiwan

Received 17 June 1997; revised 3 November 1997

Abstract

Shrinking behavior of tin oxide gels during solvent exchange in CO_2 supercritical drying was investigated. The drying process consisted of two solvent-exchanging steps, including a first replacement of water by acetone and a second of acetone by liquid CO_2. Gels prepared from a basic sol with a ζ-potential of -75 mV exhibited extensive shrinkage during both steps, while those from an acidic hydrous precipitate of lower potential ($|\zeta$-potential$| < 35$ mV) shrank only during the second step. The shrinkage during the first step correlates with the ξ-potential reduction with increasing acetone concentration, while that during the second step for both gels can be attributed to osmotic compressive pressure that arises from an increase in the liquid–solid (gel skeleton) interfacial energy with increasing CO_2 concentration. Dramatically different aerogel microstructures were obtained by controlling the gel surface potential in conjunction with different combinations of solvent-evaporating and supercritical drying. © 1998 Elsevier Science B.V.

PACS: 81.05.Hd; 81.05.Rm; 81.20.Fw; 81.40.−z; 82.70.Gg

1. Introduction

The nature of gel-shrinkage during drying is known to have a decisive effect on gel microstructure. For instance, the existence of predominantly micro-pores in oxide xerogels, that are obtained by the conventional solvent-evaporating drying process, is a consequence of the capillary force at vapor–liquid interfaces, which causes gel shrinkage and pore-size reduction. To minimize gel shrinkage supercritical drying was introduced by Kistler [1] for making oxide aerogels. There are two types of supercritical drying processes, namely the high- and low-temperature ones, that have appeared in the literature for the drying of oxide gels. In the high-temperature process, the original solvent, mostly alcohol–water mixtures, used to prepare the wet gels, is heated and pressurized to the supercritical state ($T_c = 374$°C, $P_c = 22.0$ MPa for water; 240°C, 7.93 MPa for methanol; 243°C, 6.36 MPa for ethanol [2]) and isothermally vented [3–9]. In the low-temperature process, the original solvent was replaced by another solvent, such as $CO_{2(l)}$ ($T_c = 31.1$°C, $P_c = 7.36$ MPa), which has a lower T_c [2,10–13]. A CO_2 supercritical drying process generally involves two solvent-exchanging steps, including the first replacement of the original solvent by a solvent that has high miscibility toward both the original solvent and $CO_{2(l)}$, and a second replacement of this solvent by $CO_{2(l)}$ in an autoclave. CO_2 is subsequently vented as supercritical fluid.

* Corresponding author. Tel.: +886-2 363 0231/ext. 2182; fax: +886-2 362 3040; e-mail: nlw001@ccms.ntu.edu.tw.

PII S0022-3093(97)00484-5

Previous studies showed that, when subjected to high- or low-temperature supercritical drying, oxide gels shrink [12,14,15], although less than in solvent-evaporating drying. It was observed that, while the gel dimension remained unchanged during the final $CO_{2(l)}$-venting step, significant gel shrinkage takes place during the solvent-exchange steps. A large literature devoted to the understanding of the gel shrinkage in solvent-evaporating drying, is summarized by Brinker and Scherer [16]. In contrast, there have relatively been few for supercritical drying [12,14], which focused mainly on silica and none of which concerns metal oxide gels. In this work, tin oxide particulate gels containing particles with greatly different surface potentials were subjected to the CO_2 supercritical drying that consisted of two most commonly adopted solvent-exchanging steps, including first one with water being replaced by acetone and the second with acetone by $CO_{2(l)}$. Their shrinkage behavior, along with the driving mechanisms, during the solvent-exchanging steps were investigated.

2. Experimental

Wet gel preparation by a spontaneous solution–sol–gel method has been previously described [17]. An aqua-alcoholic (H_2O/ethanol = 3:2 by volume) solution containing 0.03 M $SnCl_4.5H_2O$ was aged at room temperature without introducing any precipitating reagent. During aging, solution-to-sol and sol-to-gel transitions took place spontaneously to produce gelatinous precipitates. Once the precipitate sedimented, the supernatant solution was decanted and fresh water was replenished. The cycle consisting of consecutive aging, solution-decanting and water-replenishing steps was repeated until the solution pH value reached $\sim$4.0. The precipitate was then collected in a Teflon container and was either directly subjected to the supercritical CO_2 drying process or partially dried at 34°C under 75% humidity to produce a free-standing gel. These gels will hereafter be referred to as the acidic gels and the one without being partially dried as the fresh gel. To prepare the basic gels, ammonia was added into the solution containing the precipitate until pH reached $\sim$9.0. The white precipitate was completely peptized within 24 h into a transparent sol. Free-standing basic gels were obtained by subjecting the sols to solvent-evaporating drying under the same conditions as the acidic ones.

The CO_2 supercritical drying consisted of solvent-exchanging first with water being replaced by acetone and second with acetone by liquid CO_2. For the free-standing gels, the first solvent-exchanging step was carried out by consecutively immersing the gels in aqua-acetonic solutions with increasing acetone contents, ranging from 50% (by volume) to 100% with 10% increment between solutions. (Throughout this paper, the composition of an aqua-acetonic solution will be expressed in terms of species volume fraction calculated before mixing; i.e., the volume change, which is no greater than $\sim$3%, due to mixing is ignored.) The gel was then moved to a windowed autoclave, where the gel was immersed in an acetone bath. Fig. 1 shows the CO_2 pressure–temperature, $P(CO_2)$–T, path during the second solvent-exchanging and final supercritical drying steps. The second solvent-exchanging step was carried out by continuously flushing the autoclave with flowing $CO_{2(l)}$ for $\sim$30 min at 6.2 MPa. Slightly different procedures were adopted for handling the fresh acidic gel. In this case, the fresh wet gel, i.e., the precipitate, was directly dispersed in acetone in the first step. After the precipitate sedimented, sludge containing the precipitate and acetone was collected in a tube which has a frit attached to one end. The sludge was viscous enough to show no leakage through the frit. Then the gel along with the entire tube was

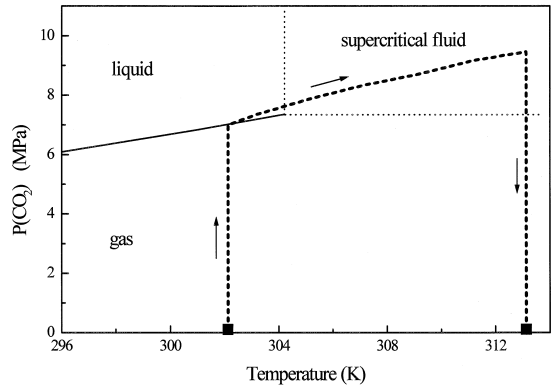

Fig. 1. The $P(CO_2)$–T diagram showing the operating path involved in the supercritical CO_2 drying process.

immersed in acetone inside the autoclave for the second solvent-exchanging step. Fresh basic gels, i.e., the sols, cannot be handled in the same manner due to its low viscosity and hence only the partially-dried, free-standing basic gels were used.

The final drying step, as indicated in Fig. 1, was carried out by raising the temperature to 40°C and the pressure simultaneously went up to ~9.6 MPa. The entire system was then allowed to equilibrate for 0.5 h and was then vented.

Photographs of gels at different stages were taken for determining shrinkage. Corrections for image distortion caused by light refraction through various liquid–liquid, liquid–solid and gas–solid interfaces were made by using objects of known dimensions. Microstructures of aerogels were characterized by using nitrogen adsorption (ASAP2000, Micromeritics) and scanning electron microscopy (SEM; Hitachi, S800). ξ(zeta)-potential was measured by using a ξ-potentiometer (Malvern, Zetamaster). The particle sizes of the sol were determined by a Malvern 4700 C particle-size analyzer, which employed a 633 nm laser incident beam and a light-scattering detector located at 90°. The particle size was calculated based on the Stoke–Einstein equation, assuming spherical solid particles.

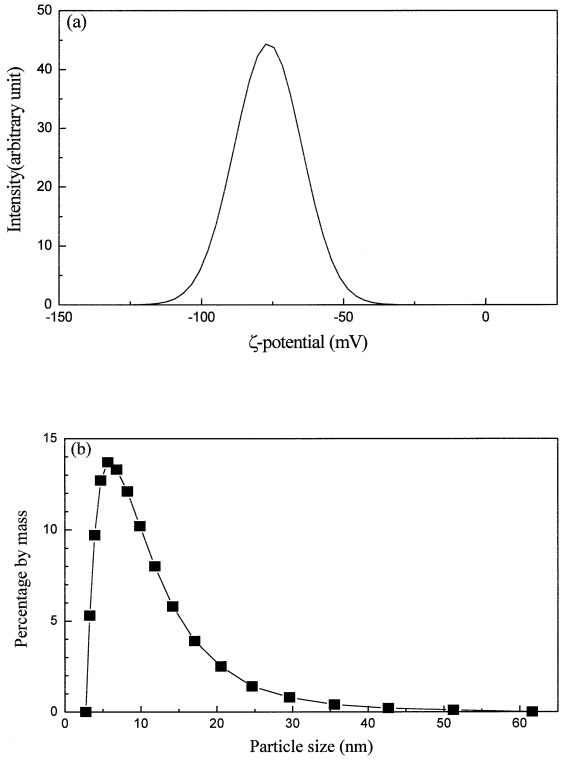

Fig. 2. The properties of the sol from which the basic gels are made. Shown are (a) ξ-potential distribution curve; (b) particle size distribution.

3. Results

Acidic wet gels, prepared from the gelatinous precipitate with pH = 4.0, are opaque, apparently consisting of large coagulated masses that effectively scatter visible light. Basic gels obtained from sols at pH = 9.0 are transparent. The ξ-potential measurements of the sol gave a potential distribution that had an average potential of ~ −75 (±3) mV (Fig. 2a), while light scattering measurement of the sol showed a narrowly distributed particle-size distribution that peaked at ~60 Å with 85% (in mass) having a size less than 200 Å (Fig. 2b). ξ-potential measurements were also conducted on the solutions containing diluted acidic precipitate but the data widely scattered over the range between −13.5 and −35 mV, presumably because the acidic precipitates easily coagulate. They, however, serve to demonstrate the fact that the ξ-potential of the acidic gel is indeed rather smaller than that of the basic sol.

In addition to their different appearances, the acidic and basic gels exhibited different shrinking behaviors during the solvent-exchanging steps (Table 1). When the fresh acidic gel was loaded in a test tube and immersed in acetone bath, no shrinkage was observed. Nor has shrinkage taken place when the partially-dried acidic gels were subjected to the standard first-step solvent-exchanging procedures. Significant gel shrinkage, however, took place for all the acidic gels during the second step (Table 1, samples A-0 ~ 2). The basic gels exhibited shrinkage during both solvent exchanging steps (Table 1, samples B-1 and 2). In all cases, the shrinkage taking place during the first step is far more extensive than that during the second step. For the former, more than one-half of the overall shrinkage occurred when the gels were finally immersed in pure acetone (after being previously washed in a 90%-acetone solution).

ξ-potential measurements were carried out on basic sols dispersed in aqua-acetonic solutions of dif-

Table 1
Gel shrinkage during the solvent-exchanging steps

Sample no.	Period of pre-drying[a] (h)	Shrinkage $(-\Delta L/L_0)$[b] by solvent-exchanging	
		1st step	(1st + 2nd) step
A-0	0	0.0	25%
A-1	24	0.0	8.0%
A-2	48	0.0	7.0%
B-1	24	25%	30%
B-2	48	11%	16%

[a] Pre-drying was carried out at 34°C under 75% humidity.
[b] $-\Delta L/L_0$: the axial linear shrinkage with respective to the gel dimension, L_0, after pre-drying and before any solvent-exchanging procedure.

ferent acetone concentrations. These solutions were introduced with the same concentration of ammonia as that used in peptizing the basic sol, showing approximately the same pH value (8.5–9.0). It was found that, with increasing acetone concentration, the ξ-potential first showed a gradual decrease up to 90%-acetone, followed by a rapid drop to ~ -30 mV in pure acetone (Fig. 3).

During the second-solvent exchanging step, as indicated in Fig. 1, CO_2 was introduced into the autoclave originally as a gas and, when the dew point was reached, as a liquid. Dissolution of CO_2 into the acetone was evidenced by the presence of a 'finger-pattern' flow. Simultaneously, the gel shrinkage, for both acidic and basic gels, commenced from the top and propagated to the bottom, in the same direction as that of the CO_2 flow. In a set of experiments, CO_2 pressure was increased step-wise and the gel dimension was monitored in situ. Fig. 4a shows the dynamics of shrinkage of a fresh acidic gel. As shown, with each step-increase in CO_2 pres-

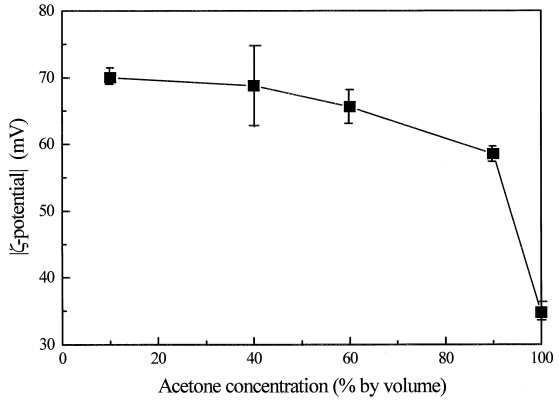

Fig. 3. $|\xi$-potential$|$ of the basic sol as a function of acetone concentration in water–acetone solutions.

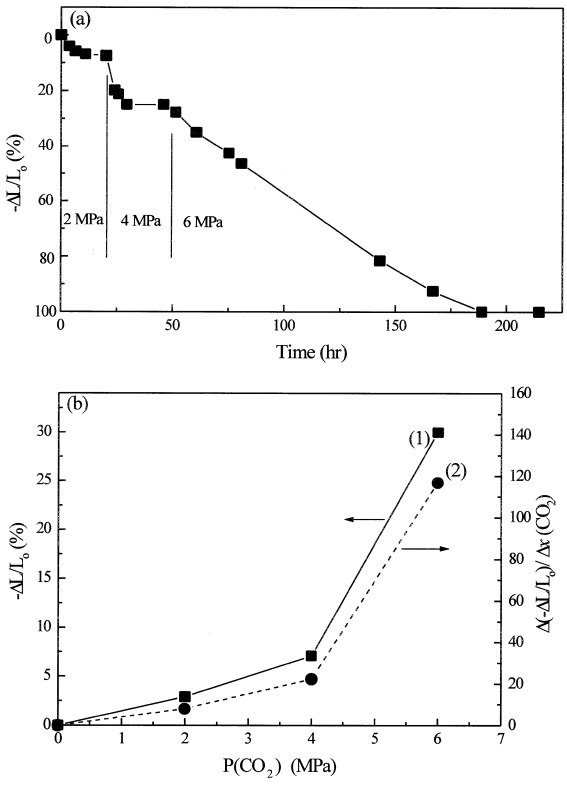

Fig. 4. Shrinking behaviors of the fresh acidic gel under pressurized CO_2. Shown are (a) the dynamics of shrinkage $(\Delta L/L_0)$ upon step-increase (2 MPa) in CO_2 pressure; and (b) overall shrinkage (■) and shrinkage caused by unit increment in CO_2 molar fraction, $\Delta(-\Delta L/L_0)/\Delta x(CO_2)$, (●) as a function of CO_2 pressure, $P(CO_2)$.

sure, the gel dimension first decreased sharply and then leveled off. Both the plateau shrinkage and the shrinkage caused by unit increment in CO_2 molar fraction, i.e., $\Delta(-\Delta L/L_0)/\Delta x(CO_2)$, increase with $P(CO_2)$ (Fig. 4b). (The CO_2 molar fractions, $x(CO_2)$, are calculated from Ref. [18]). The total shrinkage in this case is $\sim 40\%$, which is greater than that encountered in the drying process. That is, a slower pressurizing protocol results in a greater shrinkage.

In all runs, the gel dimension was eventually stabilized during purging of the autoclave with $CO_{2(l)}$ at 6.2 MPa and remained unchanged during the final heating and venting steps. The aerogels, however, further slowly shrank during its retention in a dry box (relative humidity $\sim 25\%$). Table 2 summarizes the nitrogen adsorption data of resulted aerogels, while Fig. 5 showed the BJH pore size distributions of the acidic and basic aerogels that have been subjected to one or two days of pre-drying prior to supercritical drying. (The terms 'acidic aerogels' and 'basic aerogels' simply refer to the aerogels prepared from the acidic and basic gels, respectively.) Data of xerogels (Sample A-*X* and B-*X*) were also included for comparison. For aerogels having been subjected to the same period (up to two days) of pre-drying, the basic aerogels have a much higher density, and hence a more compact structure, than the acidic ones. Furthermore, within the meso- and micro-pore regions, the pore size distributions are much narrower in the basic aerogels (Fig. 5). The dramatic differences in their apparent densities (column 2, Table 2) resulted from different amounts of macro-

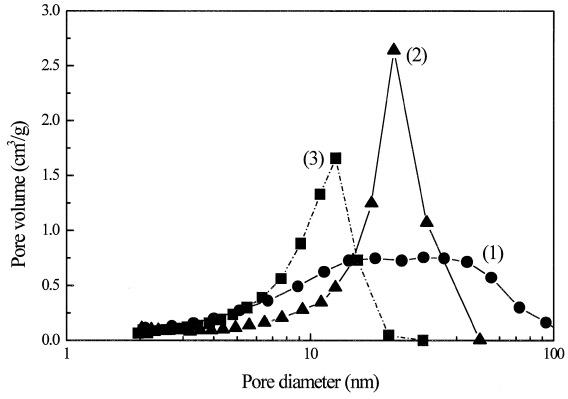

Fig. 5. The BJH adsorption pore size distributions of (curve 1) the acidic aerogel having been subjected to 48 h of pre-drying; (2) basic aerogel; 24 h; (3) basic aerogel; 48 h.

pores therein. The presence of macro-pores, with a diameter greater than 0.1 μm, which cannot be accurately measured by adsorption, was evidenced in both aerogels by SEM studies. The macro-pore volume was estimated as follows. Sintering and SEM studies, of which the detail will be reported elsewhere, have shown that the xerogels contain negligible amount ($< 5\%$ in total volume) of macro-pores and, as calculated from their bulk density and pore volumes, have a skeleton density of ~ 4.3 g/cm^3. By assuming that the solid phase in the aerogels has the same skeleton density as that in the xerogels, the total pore volumes were calculated. The differences between calculated and measured pore volumes were attributed to the macro-pore volumes, which are

Table 2
Microstructural data of the tin oxide aerogels

Sample #	Apparent density[a] (g/cm^3)	BET surface area (m^2/g)	Single-point pore volume V_p (cm^3/g)	Macro-pore volume V_{mp}^b (cm^3/g)
A-0	0.11	283	0.7	8.0
A-1	0.20	290	0.76	4.0
A-2	0.53	260	0.66	1.1
A-X	3.0	210	0.11	~ 0.0
B-1	0.70	250	0.80	0.40
B-2	0.95	250	0.50	0.08
B-X	3.2	200	0.10	~ 0.0

[a] The apparent density is determined directly from the weight and dimension of the aerogel.
[b] The macro-pore volume, V_{mp}, is calculated based on a skeleton density, ρ_{sk}, of 4.3 g/cm^3 and apparent density, ρ, by $V_{mp} = [(1/\rho) - (1/\rho_{sk})] - V_p$.

listed in Table 2 (column 5). Macro-pores were found to prevail in all the acidic aerogels (with a pre-drying period of up to 2 days).

4. Discussion

The zero-charge point and isoelectric point of tin oxide in water are known to be close to pH = 4.5 [19,20]. Thus, the causes to the differences in their ξ-potentials between the acidic and basic gels are apparent. Being close to the isoelectric point, the acidic gels (pH = 4.0) are composed of coagulated particles of low surface potential. The small negative (but not positive) ξ-potential exhibited by the acidic gel at pH = 4.0 is believed to be due to adsorption of Cl^-, of which the concentration was reduced from ~ 0.1 M in the starting solution to $< 5 \times 10^{-4}$ M as the pH was adjusted to ~ 4.0. (It should be noted that it is the high Cl^- concentration that causes coagulation during the early stage of condensation, e.g., at pH = 1.0 [21].)

In contrast, being away from the isoelectric point, the basic gel (pH = 9.0) is constituted of rather uniformly distributed particles with high surface potentials. The stability of the gel structure of this sort is known to depend to a great extent on the magnitude of the electrostatic repulsive forces acting between particles. As shown in Fig. 3, as the solution pH and ion concentration were kept approximately constant, the ξ-potential of the basic sol showed a monotonous decrease with increasing acetone concentration. In particular, the rapid reduction between 90% and 100%-acetone solutions correlates very well with the observation that shrinkage during the first step takes place most significantly over the same concentration range. By DLVO theory [19], a reduction in ξ-potential (together with a smaller solution dielectric constant [22,23]) will lead to a decrease in interparticle repulsive force at the same interparticle distance, causing gel to shrink. This is also consistent with the fact that the acidic gels, in which the particles originally have low surface potentials, did not show shrinkage during this step.

The reduction in ξ-potential and hence in repulsive force during the first step can be reasoned in several ways, in terms of the changes in solution properties. For instance, as the solution dielectric constant decreases with increasing acetone concentration [22,23], the double layer is compressed. That is, the electrostatic potential drops more rapidly with distance from the particle surface. Added to that, dilution in $[OH^-]$ by solvent-exchanging is expected to result in reduction in surface potential. The dramatic potential reduction observed between 90 and 100% acetone signals severe reconstruction of the Stern layer structure. Reasoned along the line of Langmuir adsorption, the reconstruction is likely to result from the transition from saturated to undersaturated regions for water adsorption.

The non-shrinkage behavior of the acidic gels during the first step gives a clear indication that balance in interparticle forces cannot be a critical factor to account for their shrinkage during the second step. Basic gels after the first step have a ξ-potential comparable to that of the fresh acidic gels (Fig. 3) and are expected to behave similarly.

Hydrous oxide gel is known to contain large amount of polar and charged species. The skeleton surface is covered with a high-density of neutral or de-protonated hydroxyl surface groups. There exist layers of water molecules hydrogen-bonded to the surface groups and among themselves. Ions, such as H^+, OH^- and Cl^- ions, are also embedded within the water layers, interacting with the surface via electrostatic and van der Waals forces. Due to the strong adsorbent–adsorbate interactions, these adsorbed species can not be completely removed even in pure acetone. Being a non-polar solvent, $CO_{2(l)}$ does not support ionic charge and is expected to have limited affinity toward molecules and groups, such as OH, with a strong dipole moment. Thus, as the CO_2 concentration increases, the ability for the acetone/CO_2 solution to accommodate these polar/charged species is expected to decrease, and hence the liquid–solid interfacial energy increases.

Accordingly, as the CO_2 concentration increases, the gel will tend to expel liquid from inside, creating an osmotic compressive pressure, in order to reduce the interfacial area. Similar mechanism has been known to contribute enormous volume change in some polymer gels [24]. The higher the CO_2 concentration, the greater the compressive pressure. This explains why, as shown in Fig. 4b (curve 1), the shrinkage increases with $P(CO_2)$. Furthermore, in

the case where $\partial\gamma/\partial x$, where γ is the interfacial tension and x the solute (in this case, CO_2) concentration, increases with solute concentration, a greater increase in the compressive pressure will be created by unit increment in the solute concentration. This explains why, as also shown in Fig. 4b (curve 2), $\Delta(-\Delta L/L_0)/\Delta x$ increases with $P(CO_2)$.

Strictly speaking, change in interfacial energy may also occur during the first step. However, in view of the good affinity of acetone toward most of the surface polar/charged species, as indicated by high solubilities of water and most hydroxide and chloride salts in acetone, the change will be much smaller than that caused by CO_2 and the compressive pressure, if exists, may be too small to cause shrinkage.

The microstructural differences between the acidic and basic aerogels are dramatic (Fig. 5 and Table 2). In addition to their original gel networks, the shrinkage mechanisms discussed above must have contributed to some extent to the differences. Microstructures are similar among xerogels, dried solely by solvent-evaporating drying. Acidic gels have a wide pore size distribution. According to the osmotic-compression mechanism discussed above, the smaller pores, which have a higher surface-to-volume ratio, will contract first, i.e., at lower $P(CO_2)$, and also experience a greater compressive pressure under the same $P(CO_2)$ and $\Delta x(CO_2)$. This causes a greater shrinkage within the coagulated masses than between the masses, leaving large voids (macropores) preferentially between the masses. For basic gels, the shrinkage during the first solvent-exchanging step allows particles to slide freely and homogeneously into a more compact configuration, giving a narrow pore size distribution. These pores are expected to behave similarly during the second-step and the uniformity is retained.

Both the potential-reduction and osmotic-compression mechanisms are solution-driven processes. Gel shrinkage by these mechanisms is expected to commonly occur in the low-temperature supercritical drying process, during which, being the nature of the process, either the solution dielectric constant or solvent dipole moment is consecutively reduced during the solvent-exchanging steps. Extensive shrinkage of the acetone-washed tin oxide gels has also been observed when they were subjected either to pressurized ethane or to liquid hexane at ambient pressure.

5. Conclusion

(1) When tin oxide particulate gels are subjected to CO_2 supercritical drying, significant gel shrinkage takes place during the solvent-exchanging steps and the shrinkage depends strongly on the particle surface potential.

(2) Two shrinkage-driving mechanisms are identified. First, reduction in interparticle repulsive force causes shrinkage of gels with high surface potential. Secondly, osmotic compressive pressure arises from increasing solution–solid(gel skeleton) interfacial energy with CO_2 concentration causes shrinkage of gels with low potential. Both mechanisms are likely to commonly occur for supercritical drying of other oxide gels using the same (CO_2) or other nonpolar solvents.

(3) A wide range of microstructures differing in both pore size distribution and average value can be achieved by controlling surface potential of the gel in conjunction with different combinations of solvent-evaporating and supercritical drying processes.

Acknowledgements

This work is supported by the National Science Council of Republic of China under contract number of NSC 85-2214-E-002-013.

References

[1] S.S. Kistler, Nature 127 (1931) 741.
[2] P.H. Tewari, A.J. Hunt, K.D. Lofftus, Mater. Lett. 3 (1985) 363.
[3] S.S. Kistler, J. Phys. Chem. 36 (1932) 52.
[4] T. Woignier, J. Phalippou, J. Zarzycki, J. Non-Cryst. Solids 63 (1984) 117.
[5] S. Komarneni, R. Roy, U. Sclvaraj, P.B. Malla, E. Breval, J. Mater. Res. 8 (1993) 3163.
[6] J. Phalippou, T. Woignier, M. Prassas, J. Mater. Sci. 25 (1990) 3111.
[7] R.A. Laudise, D.W. Johnson Jr., J. Non-Cryst. Solids 79 (1986) 155.

[8] M. Prassas, J. Phalippou, J. Zarzycki, J. Mater. Sci. 19 (1984) 1656.
[9] J.G. van Lierop, A. Huizing, W.C.P.M. Meerman, C.A.M. Mulder, J. Non-Cryst. Solids 82 (1986) 265.
[10] F. Chaput, H. Dunn, P. Fuqua, K. Salloux, J. Non-Cryst. Solids 188 (1995) 11.
[11] M.J. van Bommel, A.B. de Haan, J. Mater. Sci. 29 (1994) 943.
[12] S.Y. Kim, K.D. Nam, S.H. Ahn, K.P. Yoo, K.H. Lee, in: Proc. 3rd Int. Symp. on Supercritical Fluids, G. Brunner, P. Perrut (Eds.), vol. 3, Strasbourg, France, Oct. 17–19, 1994, p. 303.
[13] J.M. Moses, R.J. Willey, S. Rouanet, J. Non-Cryst. Solids 145 (1992) 41.
[14] T. Woignier, J. Phalippou, J. Non-Cryst. Solids 93 (1987) 17.
[15] U. Janosovits, G. Ziegler, U. Scharf, A. Wokaun, J. Non-Cryst. Solids 210 (1997) 1.
[16] C.J. Brinker, G.W. Scherer, Sol–Gel Science, Academic Press, New York, 1990.
[17] N.L. Wu, L.F. Wu, Y.C. Yang, S.J. Huang, J. Mater. Res. 11 (1996) 813.
[18] C.J. Chang, C.Y. Day, C.M. Ko, K.L. Chiu, Fluid Phase Equilibr. 131 (1997) 243.
[19] J. Hunter, Zeta-potential in Colloidal Science – Properties and Applications, Academic Press, London, 1981, p. 229.
[20] M. Ocaña, E. Matijevic, J. Mater. Res. 5 (1990) 1083.
[21] R.S. Hiratsuka, S.H. Pulcinelli, C.V. Santilli, J. Non-Cryst. Solids 121 (1990) 76.
[22] CRC Handbook of Chemistry and Physics, 69th ed., R.C. Weast, M.J. Astle, W.H. Beyer (Eds.), CRC, Boca Raton, FL, 1988.
[23] G. Åkerlöf, J. Am. Chem. Soc. 54 (1932) 4125.
[24] T. Tanaka, Sci. Am. 244 (1981) 124.